Whipping of electrified liquid jets

Josefa Guerrero[a,1], Javier Rivero[b], Venkata R. Gundabala[a,2], Miguel Perez-Saborid[b], and Alberto Fernandez-Nieves[a,3]

[a]School of Physics, Georgia Institute of Technology, Atlanta, GA 30332; and [b]Departmento de Ingenieria Aereoespacial y Mecanica de Fluidos, University of Sevilla, Sevilla 41092, Spain

We apply an electric field to a moderately conducting liquid surrounded by another coflowing liquid, all inside a glass-based microfluidic device, to study nonaxisymmetric instabilities. We find that the bending of the electrified jet results in a steady-state, helicoidal structure with a constant opening angle. Remarkably, the characteristic phase speed of the helicoidal wave only depends on the charge carried by the jet in the helicoidal region and its stability critically depends on the properties of the coflowing liquid. In fact, the steady-state helical structure becomes chaotic when the longest characteristic time is that of the inner liquid rather than that of the outer coflowing liquid. We also perform a numerical analysis to show that the natural preference of the jet is to adopt the conical helix structure observed experimentally.

instability | charged jets | electro-coflow | electrospinning

Aliquid with finite electrical conductivity in the presence of a strong electric field can deform and adopt a conical shape resulting from the balance between electric and surface tension stresses (1). However, near the apex of the cone, this structure is not stable and the associated singularity is replaced by a thin jet (2–6). The resultant cone–jet structure, which is stable within certain values of the applied voltage and imposed liquid flow rate, is the workhorse of electrospray and all its associated applications (7–10).

The jet that emanates from this structure always breaks into spherical droplets due to axisymmetric instabilities (11–13). However, in many cases, the jet bends off-axis due to a lateral instability that results from the electrostatic repulsion between bent and straight parts of the jet (14–19). If the growth rate associated to this whipping instability is larger than that associated to jet breakup, the off-axis movement of the jet becomes the most significant aspect of its evolution. This is exploited in electrospinning, where the simple liquid is replaced by a polymer solution whose solvent evaporates before drop breakup takes place, thus resulting in the formation of polymer fibers (14, 17, 18, 20). The presence of the lateral instability in this application results in thinner fibers, as bending stretches, concomittantly thinning the jet (20). Unfortunately, in most experimental realizations, whipping manifests in a chaotic fashion (15, 16, 18, 19, 21, 22) preventing us from knowing and unraveling its detailed structure and properties.

In this work, we apply an electric field to a moderately conducting liquid surrounded by a coflowing liquid to generate a steady-state whipping structure, which we find is helicoidal, with an amplitude that increases linearly along the downstream direction. Interestingly, the characteristic phase speed of the helical wave is determined by the electrostatic repulsion between the fluid elements of the jet in the whipping region. By performing a numerical analysis, we show that the conical helix structure is the natural configuration of electrified jets, provided the growth rate associated with jet breakup is small. This is true even in the absence of a coflowing liquid. However, the properties of this liquid dramatically affect the stability of the whipping structure.

We use a microfluidic device consisting of a glass capillary with a square cross-section of inner side $a = 2$ mm and two cylindrical glass capillaries with similar outer diameter, coaxially aligned with the square one; the device is similar to that used for generating double emulsions (23). One of the two cylindrical capillaries is tapered into a tip with inner diameter $d_{tip} = 47$ μm. We pump a conducting liquid, ethylene glycol, with electrical conductivity

$K = 10^{-4}$ S/m and viscosity $\eta_i = 17$ cP, through the inside of this capillary, and a dielectric liquid, polydimethylsiloxane oil, with viscosity $\eta_o = 1.5$ cP, through the voids left between the outer square cross-section and the inner circular cross-section of this capillary, as shown in Fig. 1A. The third liquid is also an electrical conductor and flows through the inside of the second cylindrical capillary. As a result of the imposed flow, the exit of the device is provided by the voids left between the outer square cross-section and the circular cross-section of this second cylindrical capillary, as also shown in Fig. 1A. To apply the external electric field, we establish an electric potential difference between the metallic needles in contact with the inner and third liquids, which due to their finite electrical conductivity act as electrodes. Using this electro-coflow configuration, we fix the flow rate of the dielectric liquid to $q_o = 60$ mL/h and adjust the flow rate of the third liquid to maintain a constant tip-to-counter-electrode distance of $L = 2.2$ mm. We then vary the inner-fluid flow rate, q_i, and the applied voltage, V, to obtain a steady-state whipping structure, which we monitor using high-speed imaging and optical microscopy. We also measure the electric current, I, using a picoammeter.

The resulting time sequence of the images indicates that the whipping structure is 3D, with regions that are in and out of focus, as shown in the Movie S1 and in agreement with previous results (16–19, 21, 22). It also has a wavelike character with propagation direction along the axial direction. Finally, we find that the whipping structure has a constant opening angle, α, reflecting the linear increase of the lateral amplitude of the instability along the axial direction.

Significance

Whipping is a lateral instability experienced by charged jets and exploited in electrospinning to make polymer fibers. In contrast to its axisymmetric, Rayleigh–Plateau counterpart, which induces jet breakup and drop formation, whipping is nonaxisymmetric and manifests itself in a chaotic fashion, with the jet moving in uncontrolled and hardly quantifiable ways. As a result and despite its physical significance, we still do not know its detailed structure and properties. Here we perform microfluidics experiments to generate and study steady-state whipping. Remarkably, when the longest characteristic time scale in the problem is that of the surrounding liquid, the whipping structure is steady and helicoidal. Otherwise, it is as chaotic as it was in all previous studies.

APPLIED PHYSICAL SCIENCES

Fig. 1. (A) Schematic of the electro-coflow device. (B) Representative image of the whipping structure. (C) Helicoidal trajectory for $\alpha = 46.29$, $\overline{\lambda} = 25.26\,\mu m$, and $T = 192.3\,\mu s$. The x, y, and z scales are in micrometers. (D) The yz and (E) xy projections of (F) the whipping trajectory obtained from the numerical analysis for $Re^{(i)} = 0.056$, $L/d_{tip} = 88$, $2\varepsilon V^2/(\gamma d_{tip}) = 654$, $4\eta_i q_i/(\pi\gamma d_{tip}^2) = 0.028$, and $d_{tip}I/(4q_i) = 0.0056$. The x, y, and z scales are made dimensionless with L.

Based on these results, we hypothesize that the structure is that of a helix with a linearly increasing amplitude. Hence, in terms of the time, t, the parametric equations of the structure in Cartesian coordinates are:

$$x(t) = \frac{\overline{\lambda} t}{T} \tan\left(\frac{\alpha}{2}\right) \cos\left(\frac{2\pi t}{T}\right), \qquad [1]$$

$$y(t) = \frac{\overline{\lambda} t}{T} \tan\left(\frac{\alpha}{2}\right) \sin\left(\frac{2\pi t}{T}\right), \qquad [2]$$

$$z(t) = \frac{\overline{\lambda} t}{T}, \qquad [3]$$

with $\overline{\lambda}$ the mean wavelength obtained by averaging the distance between consecutive minima and consecutive maxima (Fig. 1B), and T the period measured by correlating consecutive images and identifying the snapshots with the largest overlap. To obtain representative values of these quantities at each V and q_i, we average them using 100 independent measurements. For $V = 1{,}800$ V and $q_i = 80$ μL/h, we obtain $\alpha = (46.29 \pm 0.12)°$, $\overline{\lambda} = (25.26 \pm 0.07)\,\mu m$, and $T = (192.3 \pm 0.1)$ μs, and the reconstructed whipping structure based on Eqs. 1–3 shown in Fig. 1C.

To test our hypothesis, we recall that a helicoidal trajectory results from the composition of uniform motion in the axial direction, which we take as the z direction, and circular motion in the perpendicular xy plane, and measure the component of the velocity in this plane, $v_{rad}^{exp} = 2\pi A(z)/T$, at certain axial location, with $A(z)$ the amplitude of the whipping structure at that

location. We obtain $v_{rad}^{exp} = O(0.1$ m/s$)$. For the same axial position, we use Eqs. 1 and 2 to estimate this speed: $v_{rad}^{est} = |\dot{x}\,\hat{i} + \dot{y}\,\hat{j}|$, where $\hat{i}$ and $\hat{j}$ are the unit vectors in the x and y directions, respectively. We find that $v_{rad}^{exp} \simeq v_{rad}^{est}$, as shown in Table 1 for representative values of q_i and V, confirming the helicoidal character of the experimental whipping structure.

We can also experimentally determine the axial component of the whipping velocity, which is nothing but the phase velocity of the wave: $v_{phase}^{exp} = \overline{\lambda}/T$. We obtain $v_{phase}^{exp} = O(0.1$ m/s$)$, as also shown in Table 1. To account for this value, we consider that the axial motion is uniform. We then divide the jet in fluid elements of length equal to the jet diameter and balance the axial component of the electric force acting on a fluid element due to all other fluid elements in the whipping region, $F_{el,z}$, with the axial component of the drag force exerted on that element by the outer viscous liquid, $F_{drag,z}$. Hence, $F_{el,z} = F_{drag,z}$, where

$$F_{el,z} = \frac{1}{4\pi\epsilon}\left(\sum_{i\neq j}\frac{Q^2}{r_{i,j}^3}\vec{r}_{i,j}\right)\cdot\hat{k}, \qquad [4]$$

$$F_{drag,z} = \frac{4\pi\eta_o d_j}{\log(1.64)}\left(\vec{v} - \vec{v}_o\right)\cdot\hat{k}, \qquad [5]$$

with $\vec{v}$ as the velocity of the fluid element, ε and $\vec{v}_o$ as the dielectric permittivity and average velocity of the dielectric liquid, Q as the charge of the fluid element, $r_{i,j}$ as the distance between fluid elements i and j, and $\hat{k}$ as the unit vector in the z direction. We obtain Q from the electrical current, assuming the charge carried by the jet in the whipping region is mostly at the surface and convected by the flow (24). In this case, $Q = I\pi d_j^3/(4q_i)$, with d_j as the jet diameter, which we can measure accurately before the whipping region, as shown in Fig. 1B. For $\vec{F}_{drag}$, we use the drag on a finite cylinder of length and diameter d_j, located perpendicular to the flow (25). From the force balance at each fluid element, we obtain the axial component of $\vec{v}$ at each axial location z. The average of all these axial values provides an estimate of the phase speed, v_{phase}^{est}, which is of the same order of magnitude of the experimental measurement, as shown in Table 1. This agreement indicates that the phase speed of the whipping structure is determined by the charge carried by the jet. In this case, the effect of the imposed V and q_i on the whipping structure is to set the value of Q, which is what ultimately affects the properties of the jet in the whipping region.

We note that the phase speed depends weakly on z; it decreases with increasing z up to certain axial position, as shown in Fig. 2A. This implies that, in this region, the axial distance traveled by the whipping wave in time T should decrease. Consistent with this, we find that the whipping wavelength always slightly decreases with z; this can be seen in the example shown in Fig. 1B and has also been reported by other authors (22).

Our results conclusively show that the whipping structure is helical, emphasizing the importance of the lateral unstable modes leading to this shape. To test this, we perform a numerical analysis of a straight jet of length l with surface charge density σ, diameter d_j,

Table 1. Experimental and estimated values of the xy plane and phase velocities in meters per seconds for certain V and q_i

q_i (μl/h)	V(V)	v_{rad}^{exp}	v_{rad}^{est}	v_{phase}^{exp}	v_{phase}^{est}
35	1,800	0.1	0.03	0.07	0.2
50	1,950	0.09	0.06	0.09	0.2
80	2,250	0.1	0.2	0.2	0.1
140	2,400	0.08	0.1	0.05	0.04

The values of v_{rad} correspond to $z = 20.9$ μm; similar agreement is obtained at other z.

Guerrero et al.
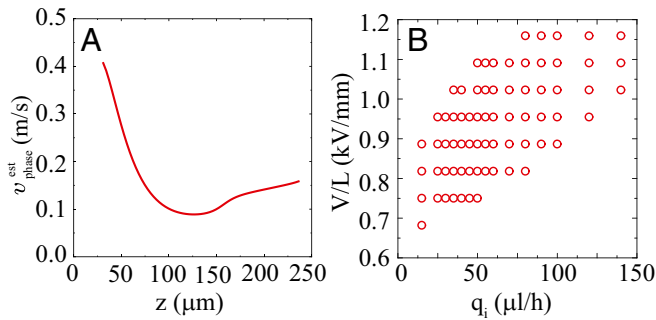
Fig. 2. (A) Estimated phase velocity, v_{phase}^{est}, as a function of the axial coordinate z for $V = 1{,}950$ V and $q_i = 90$ μL/h. (B) State diagram in the V/L - q_i representation where steady-state whipping is observed. $q_o = 60$ mL/h; $\eta_o = 1.5$ cP.

inner speed at the injection needle $u_i = 4q_i/(\pi d_{tip}^2)$, viscosity η_i, and density ρ, in the presence of an external electric field $\vec{E} = V/L\,\hat{k}$. Note that we do not consider the presence of an outer fluid medium. In addition, because the jet is slender, we simplify our problem to a single dimension by averaging all quantities over the jet cross-section. We then use Cosserat's rod theory (26, 27) or its equivalent for liquid jets (28, 29), which is expressed in terms of a curve that specifies the center of the circular cross-section and an orthonormal triad characterizing its orientation in space, $\hat{d}_1$, $\hat{d}_2$, and $\hat{d}_3$, where $\hat{d}_3$ is the unit vector tangent to the centerline s at every position. The velocity field is expressed as $\vec{v} = \vec{c} + u\hat{d}_3$, where $u\hat{d}_3$ is the relative velocity of the fluid with respect to that of the center line, $\vec{c} = \partial_t \vec{r}$, with $\vec{r}$ the position vector of the center line. The equations of motion can be obtained from balances of mass, linear and angular momentum applied to a control volume moving with the center line. The mass conservation equation is:

$$\frac{\partial A}{\partial t} + \frac{\partial}{\partial s}(uA) = 0, \qquad [6]$$

where $A = \pi d_j^2/4$ is the jet cross-section. The linear momentum equation is:

$$\frac{\partial \vec{f}}{\partial s} + \pi\gamma\frac{\partial\left(d_j\,\hat{d}_3\right)}{\partial s} + \vec{\tau}_e = \rho A\frac{d\vec{v}}{dt}, \qquad [7]$$

where $d/dt = \partial/\partial t + u\partial/\partial s$ is the material derivative. The vector $\vec{f}$ is a force related to viscous and surface tension stresses, which we write using Trouton's model (30):

$$\vec{f}\cdot\hat{d}_3 = 3\eta_i A\frac{\partial u}{\partial s} - \pi\gamma\frac{d_j}{2}. \qquad [8]$$

Recall that in the one-dimensional approach we are considering, the contribution from surface tension directly appears in the force balance. The first derivative of $\vec{f}$ with respect to s is related to extensional stresses, and the second term in the left-hand side of Eq. 7 is related to bending stresses. The vector $\vec{\tau}_e$ is related to the electric force exerted on a point of the centerline by the external field and due to the net repulsion resulting from the charged jet itself (16):

$$\vec{\tau}_e = \pi d_j\sigma\vec{E} - \frac{(\pi d_j\sigma)^2}{4\pi\varepsilon}\log\left(\frac{2L}{d_j}\right)\vec{\kappa}\times\hat{d}_3 \qquad [9]$$

where $\vec{\kappa}$ is a generalized curvature vector: $\vec{\kappa} = \kappa_1\hat{d}_1 + \kappa_2\hat{d}_2 + \kappa_3\hat{d}_3$, with κ_1 and κ_2 as the two curvatures of the centerline and κ_3 its torsion; $\vec{\kappa}\times\hat{d}_3$ is a vector normal to the centerline of the jet giving the direction of the self-repulsion contribution.

Finally, the angular momentum equation is:

$$\frac{\partial}{\partial s}\vec{m} + \hat{d}_3\times\vec{f} + \frac{1}{2}\gamma A\frac{\partial d_j}{\partial s}P_0\cdot\vec{\kappa} = \rho A\frac{d}{dt}\left(\frac{d_j^2}{16}P_2\cdot\vec{\omega}_c\right) \qquad [10]$$

where we have defined the tensor $P_k := \hat{d}_1\hat{d}_1 + \hat{d}_2\hat{d}_2 + k\hat{d}_3\hat{d}_3$, and $\vec{m}$ is the torque of $\vec{f}$ with respect to the center of the circular cross-section (29):

$$\vec{m} = 3\eta_i\frac{\pi d_j^4}{64}P_{2/3}\cdot\frac{\partial\vec{\omega}_c}{\partial s} \qquad [11]$$

with $\vec{\omega}_c = \vec{\omega} + u\vec{\kappa}$ the angular velocity, which we write in terms of the angular velocity in the frame of reference of the jet, $\vec{\omega}$, and a Coriolis term, $u\vec{\kappa}$. Note that the spatial and time derivatives of the unit vectors $\hat{d}_i$ are related to the curvature and angular velocity vectors: $\partial_s\hat{d}_i = \vec{\kappa}\times\hat{d}_i$ and $\partial_t\hat{d}_i = \vec{\omega}\times\hat{d}_i$. Furthermore, $\vec{\kappa}$ and $\vec{\omega}$ must satisfy the compatibility relations, $\partial_s\vec{c} = \vec{\omega}\times\hat{d}_3$ and $\partial_t\vec{\kappa} = \vec{\omega}\times\vec{\kappa} + \partial_s\vec{\omega}$, resulting from the identities $\partial_s\partial_t\vec{r} = \partial_t\partial_s\vec{r}$ and $\partial_s\partial_t\hat{d}_i = \partial_t\partial_s\hat{d}_i$.

The above equations are solved with the following boundary conditions at the injection needle, where $s = 0$, and at the end of the jet, where $s = l$: $u(0) - u_i = d_j(0) - d_{tip} = \vec{c}(0) = \vec{\omega}(0) = \vec{\kappa}(0) = 0$ and $\vec{f}(l) + \pi\gamma d_j/2\hat{d}_3 = \vec{m}(l) = 0$. Because we are mainly interested in periodic solutions, we express any vector quantity in terms of a rotation tensor around $\hat{d}_3$ as $\vec{b}(s,t) = [\cos(\Omega t)(\overline{\overline{I}} - \hat{d}_3\hat{d}_3) + \sin(\Omega t)(\hat{d}_3\times\overline{\overline{I}}) + \hat{d}_3\hat{d}_3]\cdot\vec{b}(s,0)$, where Ω is the jet rotation frequency around the axial direction and $\vec{b}$ stands for either $\vec{v}$, $\vec{\omega}$, $\vec{\kappa}$, $\vec{f}$, or $\vec{m}$. Observe that this ensures that the $\hat{d}_3$ component of the vector remains invariant along the orbit, and its projection on the $\hat{d}_1$–$\hat{d}_2$ plane changes periodically. In addition, we note that the scalar quantities u and d_j retain their initial value: $u(s, t) = u(s, 0)$ and $d_j(s, t) = d_j(s, 0)$. With these considerations the time dependence disappears from the original equations, hence resulting in a nonlinear boundary value problem in the spatial variable s. We note that our model correctly considers momentum balance in all sections of the jet, in contrast to previous models (16, 19). In addition, we solve the full nonlinear model and do not simply perform a stability analysis of a base state of the jet.

To solve the problem, we first find the periodic solution corresponding to a set of q_i and V values for which the jet is nearly straight. Then, we smoothly change the values of these parameters in a way that the solution corresponding to a given set can be used as initial guess to iterate the solution corresponding to the next one. For $q_i = 80$ μL/h and $V = 1{,}800$ V, we obtain a conical helix, as shown in Fig. 1 D–F, with $\alpha = 40°$ and $1/\Omega = T = 102$ μs, consistent with the experimental results.

The agreement between the model and the experiment can be understood by comparing the relative importance of the forces considered in the model. Considering that the typical speed $u \sim 0.1$ m/s and taking d_j, V/L, $1/d_j$, and L/u, as characteristic arc length, external electric field, curvature, and time, respectively, we find that the dominant force in the problem is that associated to the electrostatic self-repulsion of the jet, which is exactly what we found was the key ingredient to understand the experimental value of the phase speed of the helical wave.

Interestingly, although in most experimental studies the whipping structure is either chaotic and uncontrolled (15, 16, 19) or it is only able to persist for a very narrow range of V and q_i values (22), in our experiments the steady-state whipping structure persists over an extended range of operating parameters, as shown in Fig. 2B. Because most of the other experiments are performed in the presence of quiescent air or hexane, this discrepancy suggests that it is the presence of the more viscous outer liquid in our experiments what ultimately controls the range in parameter space where steady-state whipping is

APPLIED PHYSICAL SCIENCES

observed. To explore this possibility, we compare the values of the relevant dimensionless numbers: the Reynolds number, $Re = t_i/t_v$; the Weber number $We = (t_i/t_c)^2$; the Ohnesorge number $Oh = t_v/t_c$, $S_1 = (t_c^{(o)}/t_v^{(i)})^2$ and $S_2 = (t_c^{(i)}/t_v^{(o)})^2$, which we have conveniently written in terms of the capillary time, $t_c = (\rho d_j^3/\gamma)^{1/2}$; the viscous time, $t_v = \eta d_j/\gamma$; and the inertial time, $t_i = \rho v d_j^2/\gamma$, because these are the characteristic time scales in the problem. The superscripts (o) and (i) indicate outer or inner liquid, respectively. We find that in most whipping studies (15, 16, 21, 22), $Oh^{(i)} > 1$, $We^{(i)}$, $Re^{(i)} < 1$, $S_1 < 1$, and $S_2 > 1$, implying that $t_v^{(i)} > t_c^{(i)} > t_v^{(o)}$, $t_v^{(i)} > t_c^{(i)} > t_i^{(i)}$, and $t_v^{(i)} > t_c^{(o)}$. Hence, the longest characteristic time scale in all these cases is that of the inner liquid. In contrast, in our experiments, $S_1 > 1$, $S_2 < 1$, $Oh^{(o)}$, $We^{(o)}$, $Re^{(o)} < 1$, and $Oh^{(o)}$, $We^{(o)}$, $Re^{(o)} > 1$, implying that $t_i^{(i)} < t_v^{(i)} < t_c^{(i)} < t_v^{(o)} \lesssim t_i^{(o)}$ and $t_v^{(i)} < t_c^{(o)} < t_v^{(o)}$. As a result, in our experiments, the longest characteristic time scale is that of the outer liquid. Hence, the stability of the whipping structure in the space of operating parameters could indeed result from the presence of the outer coflowing liquid.

To further test this we perform experiments with other outer liquids of viscosity $\eta_o = 0.5$ cP and $\eta_o = 9.4$ cP. As in the case of $\eta_o = 1.5$ cP, the region where we observe whipping is significantly large, as shown in Fig. 3A. However, the whipping we observe for the case of the outer liquid with smallest viscosity is highly chaotic, as shown by the snapshot in Fig. 3B and Movie S2; it is reminiscent of the whipping behavior observed in previous experiments, which were all performed in quiescent air or hexadecane. In contrast, for $\eta_o = 9.4$ cP, the structure remains helicoidal and steady, as shown by the snapshot in Fig. 3C, consistent with the results for $\eta_o = 1.5$ cP. Interestingly, for the lowest viscosity case, we find that S_1, $S_2 > 1$, $Oh^{(i)}$, $We^{(i)}$, $Re^{(i)} < 1$ and $Oh^{(o)}$, $We^{(o)} < 1$, $Re^{(o)} > 1$, implying that $t_v^{(o)} < t_i^{(i)} < t_c^{(o)}$ and $t_i^{(i)} < t_v^{(i)} \sim t_c^{(i)} \sim t_c^{(o)}$. As a result, the longest time scale of the outer liquid is, in this case, comparable to the longest time scale of the inner liquid, consistent with our prior analysis and emphasizing that the presence of the outer liquid in our experiments is critical in controlling the steady-state character of the whipping structure.

Conclusions

We have shown that the whipping structure is well described as a conical helix whose properties are determined by the charge carried by the jet; this emphasizes the importance of the charge distribution downstream from the injection needle. By performing a numerical analysis of the problem, we have confirmed that the lateral, unstable modes result in a helical shape of constant opening angle, consistent with the experiments. However, we note that our 1D (Cosserat) model assuming a constant surface charge
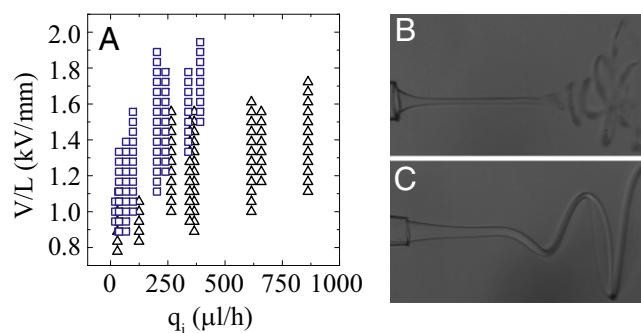
Fig. 3. (A) State diagram in the V/L - q_i representation where whipping is observed for $q_o = 17$ mL/h; (squares) $\eta_o = 9.4$ cP; (triangles) $\eta_o = 0.5$ cP. (B) Chaotic whipping structure observed for $\eta_o = 0.5$ cP, $V/L = 1.4$ kV/mm, and $q_i = 366$ μL/h. (C) Helical whipping structure observed for $\eta_o = 9.4$ cP, $V/L = 1.4$ kV/mm, and $q_i = 340$ μL/h.

density along the jet and a simplified self-repulsion due to the charge, is only the starting point for more complete models. These would ideally consider the electrohydrodynamic equations of the coupled electric and hydrodynamic problem both inside the jet and in the outside medium with appropriate boundary conditions at the interface, which is not a priori defined and should also be calculated as part of the theoretical problem.

It is worth noting that the outer coflowing liquid plays a significant role in determining the region where steady-state whipping is achieved, an interesting fact that could be exploited to obtain well-controlled jets and hence fibers, if polymer solutions are incorporated in the process. Indeed, when the largest characteristic time scale in the problem is that of the outer liquid, a helicoidal steady-state whipping structure is observed. In contrast, when the longest characteristic time scale in the problem is that of the inner liquid, whipping manifests chaotically. Thus, the presence of the outer coflowing liquid in our experiments is essential. We have, however, just begun to explore its influence. We anticipate that other distinct behaviors could result in the presence of this coflowing liquid, which were not seen before in the presence of quiescent air or in the presence of a very low viscosity quiescent liquid. It will likely be through additional experimental, computational, and theoretical work that the complete behavior of electrified jets in the presence of outer moving liquids will be unraveled and understood.

1. Taylor GI (1964) Desintegration of water drops in an electric field. *Proc R Soc Lond A* 280:383–397.
2. Fernandez de la Mora J (2007) Fluid dynamics of Taylor cones. *J Annu Rev Fluid Mech* 39:217–243.
3. Ganan-Calvo AM (2004) On the general scaling theory for electrospraying. *J Fluid Mech* 507:203–212.
4. Collins RT, Jones JJ, Harris MT, Basaran OA (2008) Electrohydrodynamic tip streaming and emission of charged drops from liquid cones. *Nat Phys* 4:149–154.
5. Cherney LT (1999) Electrohydrodynamics of electrified liquid menisci and emitted jets. *J Aerosol Sci* 30:851–862.
6. Hayati I, Bailey A, Thadros ThF (1987) Investigations into the mechanism of electrohydrodynamic spraying of liquids: II. Mechanism of stable jet formation and electrical forces acting on a liquid cone. *J Colloid Interface Sci* 117:222–230.
7. Barrero A, Loscertales IG (2007) Micro- and nanoparticles via capillary flows. *Annu Rev Fluid Mech* 39:89–106.
8. Fenn JB, Mann M, Meng CK, Wong SF, Whitehouse CM (1989) Electrospray ionization for mass spectrometry of large biomolecules. *Science* 246(4926):64–71.
9. Sill TJ, von Recum HA (2008) Electrospinning: Applications in drug delivery and tissue engineering. *Biomaterials* 29(13):1989–2006.
10. Tsai PP, Schreuder-Gibson H, Gibson P (2002) Different electrostatic methods for making electret filters. *J Electrost* 54:333–341.
11. Taylor GI (1969) Electrically driven jets. *Proc R Soc Lond A Math Phys Sci* 313:453–475.
12. Saville DA (1997) Electrohydrodynamics: The Taylor-Melcher leaky dielectric model. *Annu Rev Fluid Mech* 29:27–64.
13. Collins RT, Harris MT, Basaran OA (2007) Breakup of electrified liquid jets. *J Fluid Mech* 588:75–129.
14. Doshi J, Reneker DH (1995) Electrospinning process and application of electrospun fibers. *J Electrost* 35:151–160.
15. Hohman MM, Shin M, Rutledge G, Brenner MP (2001) Electrospinning and electrically forced jets. II. Applications. *Phys Fluids* 13:2221–2236.
16. Yarin AL, Koombhongse S, Reneker DH (2001) Bending instability in electrospinning of nanofibers. *J Appl Phys* 89(5):3018–3026.
17. Shin YM, Hohman HH, Brenner MP, Rutledge GC (2001) Experimental characterization of electrospinning: The electrically forced jet and instabilities. *Polymer (Guildf)* 42:9955–9967.
18. Rutledge GC, Fridrikh SV (2007) Formation of fibers by electrospinning. *Adv Drug Deliv Rev* 59(14):1384–1391.
19. Reneker DH, Yarin AL (2008) Electrospinning jet and polymer nanofibers. *Polymer (Guildf)* 49:2387–2425.
20. Fridrikh SV, Yu JH, Brenner MP, Rutledge GC (2003) Controlling the fiber diameter during electrospinning. *Phys Rev Lett* 90(14):144502.
21. Yang Y, et al. (2008) Effect of the electric field distribution uniformity on electrospinning. *J Appl Phys* 103:104307.
22. Riboux G, Marin AG, Loscertales IG, Barrero A (2010) Whipping instability characterization of an electrified visco-capillary jet. *J Fluid Mech* 671:226.

23. Utada AS, et al. (2005) Monodisperse double emulsions generated from a micro-capillary device. *Science* 308(5721):537–541.
24. Higuera FJ (2004) Current/flow-characteristic of an electrospray with a small meniscus. *J Fluid Mech* 513:239–246.
25. Powers TR (2010) Dynamics of filaments and membranes in a viscous fluid. *Rev Mod Phys* 82:1607–1631.
26. Champneys AR, Kuznetsov YA, Sandstede B (1996) A numerical toolbox for homoclinic bifurcation analysis. *Int J Bifurcation Chaos Appl Sci Eng* 6:867–887.
27. Goriely A, Tabor M (1997) Nonlinear dynamics of filaments I. Dynamical instabilities. *Physica D* 105:20–44.
28. Ribe NM, Habibi M, Bonn D (2006) Stability of liquid rope coiling. *Phys Fluids* 18:084102.
29. Arne W, Marheineke N, Meister A, Wegener R (2010) Numerical analysis of Cosserat rod and string models for viscous jets in rotational spinning processes. *Math Methods Appl Sci* 20:1941–1965.
30. Petrie CJS (2006) Extensional viscosity: A critical discussion. *J Non-Newt Fluid Mech* 137:15–23.

APPLIED PHYSICAL SCIENCES